

TWO NEW LONG-PERIOD HOT SUBDWARF BINARIES WITH DWARF COMPANIONS*

BRAD N. BARLOW^{1†}, SANDRA E. LISS², RICHARD A. WADE¹, AND ELIZABETH M. GREEN³

¹Dept of Astronomy and Astrophysics, The Pennsylvania State University, 525 Davey Lab, University Park, PA 16802, USA

²Department of Astronomy, University of Virginia, P.O. Box 400325, Charlottesville, VA 22904-4325, USA

³Steward Observatory, University of Arizona, 933 N. Cherry Avenue, Tucson, AZ 85721, USA

Accepted for publication in The Astrophysical Journal

ABSTRACT

Hot subdwarf stars with F–K main sequence binary companions have been known for decades, but the first orbital periods for such systems were published just recently. Current observations suggest that most have long periods, on the order of years, and that some are or once were hierarchical triple systems. As part of a survey with the Hobby–Eberly Telescope, we have been monitoring the radial velocities of several composite–spectra binaries since 2005 in order to determine their periods, velocities, and eccentricities. Here we present observations and orbital solutions for two of these systems, PG 1449+653 and PG 1701+359. Similar to the other sdB+F/G/K binaries with solved orbits, their periods are long, 909 d and 734 d, respectively, and pose a challenge to current binary population synthesis models of hot subdwarf stars. Intrigued by their relatively large systemic velocities, we also present a kinematical analysis of both targets and find that neither is likely a member of the Galactic thin disk.

Subject headings: binaries: spectroscopic — ephemerides — subdwarfs — techniques: radial velocities

1. INTRODUCTION

Mystery has shrouded the formation of hot subdwarf stars since they were first recognized as a blue extension of the horizontal branch in the Galactic halo by Greenstein & Sargent (1974) almost forty years ago. Since then, they have been found in all Galactic populations (Altmann et al. 2004; Napiwotzki 2008), globular clusters, and even the elliptical galaxy M32 (Brown et al. 2000). In this regard, it is interesting to note that the known hot subdwarfs seem to occur only in rather old populations, with ages greater than about 4–5 Gyr, and are much more common (as a percentage of the core He-burning stars) in populations with high metallicity, e.g., the old, metal-rich open clusters NGC 188 and NGC 6791 (Liebert et al. 1994; Green et al. 2006).

Models show hot subdwarf B (sdB) stars are core He-burning stars surrounded by extremely thin H envelopes, with masses around 0.5 M_⊙ and radii near 0.2 R_⊙ (Heber 1986; Saffer et al. 1994). To explain their lack of hydrogen (in contrast to other core helium-burning stars), various single-star and binary–evolution formation scenarios have been constructed, all of which entail the sdB progenitor losing its outer hydrogen envelope while on or near the red giant branch (RGB). As single-star scenarios are *ad hoc*, binary–star hypotheses have generally been favored to explain the loss of the H envelope, following early theoretical work by Mengel et al. (1976).

Han et al. (2002, 2003) presented the first results from a major binary population synthesis (BPS) study of hot subdwarf stars and described five primary formation channels, including two common envelope (CE) channels, two stable Roche lobe overflow (RLOF) channels, and the

merger of a He–core white dwarf binary. Other notable studies include those of Clausen & Wade (2011), who demonstrate that the merger of a He–core white dwarf and M dwarf can create an sdB, and Nelemans (2010), who put forth an alternative CE channel employing the γ –formalism. Many assumptions influence the outcomes in BPS models, including the common–envelope ejection efficiency, minimum mass for core He ignition, and envelope binding energy. Changing any one of these parameters, even moderately, can greatly alter the hot subdwarf population predicted by the codes. Clausen et al. (2012) recently demonstrated this sensitivity using a grid of BPS models with different inputs. They found that (1) a wide range of parameter sets can reproduce the observed subpopulation of short–period white dwarf and M dwarf binaries, which are products of CE evolution, and (2) observations of systems with F–K main sequence (MS) companions are needed to constrain the physics governing RLOF processes.

While there are numerous short–period orbits (days) published for post–CE sdB binaries (see Table A.1 of Geier et al. 2011), no definitive periods under 30 d have been reported for systems with MS companions earlier than spectral type M.³ On the contrary, long–term monitoring of these systems (Deca et al. 2012; Østensen & Van Winckel 2012; Barlow et al. 2012; Vos et al. 2012) has shown their periods are on the order of years, as originally suspected by Saffer et al. (2001) more than a decade ago. Such long periods appear to be inconsistent with the predictions of Han et al. (2002, 2003) and pose a major challenge to BPS models. Of course, orbital parameters for many more long–period systems are needed before any definitive conclusions can be drawn.

In 2005 we began monitoring the radial velocities of

* Based on observations obtained with the Hobby–Eberly Telescope, which is a joint project of the University of Texas at Austin, the Pennsylvania State University, Stanford University, Ludwig-Maximilians-Universität München, and Georg-August-Universität Göttingen.

† bbarlow@psu.edu

³ Moni Bidin & Piotto (2010) suggest that the star M5865 in globular cluster NGC 6752 is a hot subdwarf + G–K MS binary with a period of order 5 d, but details have not been published.

15 hot subdwarf stars with F–K main sequence companions at the Hobby–Eberly Telescope (HET) in order to constrain their orbital parameters. Details of this study may be found in Barlow et al. 2012 (hereafter, Paper I). Although we could only solve for the orbits of three systems using our initial data set, we presented preliminary periods for 12 targets. Almost all have periods in excess of 100 days; only two appear to have short periods, and these targets are likely hierarchical triple- or quadruple-star systems. Our preliminary results confirm previous findings that composite-spectra sdB systems tend to have long periods. To solve for the orbits of the remaining systems, we began collecting follow-up observations with the High Resolution Spectrograph on the HET in Mar 2012. An up-to-date orbital period histogram of all hot subdwarf binaries (Fig. 5 of Paper I) shows a clear dichotomy between systems with F–K main sequence companions ($P > 100$ d) and those with white dwarf or M dwarf companions ($P < 100$ d). A possible period gap is emerging around $P \sim 100$ d, but the statistics are presently too poor to claim this feature as real.

Here we present new spectroscopic observations of the sdB+MS binaries PG 1449+653 ($V=13.6$) and PG 1701+359 ($V=13.2$). We find orbital periods exceeding two years for both targets, a result in line with other sdB+F/G/K binaries. Intrigued by their relatively large systemic velocities, we combine our spectroscopy with proper motion measurements to calculate Galactic orbits and find that neither system is likely a member of the Galactic thin disk.

2. OBSERVATIONS & REDUCTIONS

From 2005 to 2008 we monitored PG 1449+653 and PG 1701+359 spectroscopically with the Medium-Resolution Spectrograph (MRS; Ramsey et al. 1998) on the Hobby–Eberly Telescope (HET). Full details on the observational setup used may be found in Paper I. We commenced follow-up observations in 2012 with the High Resolution Spectrograph (HRS) on the HET, using the 2" optical fiber pair, the 316 mm⁻¹ cross-disperser grating, and 2×3 on-chip binning to achieve an average resolution of $R=30,000$ over the 4076–7838 Å spectral range. This configuration yields an average dispersion of ~ 3.6 km s⁻¹ per binned pixel and samples ~ 2.7 pixels per resolution element. Target spectra were taken in pairs and later combined to help remove cosmic rays. Standard calibration frames were also collected each night using the same instrumental setup, including twilight sky spectra, bias frames, quartz lamp flatfield spectra, and, on most occasions, spectra of telluric, RV, and spectrophotometric standard stars.

We bias-subtracted and flat-fielded all HET data using the *ccdproc* routine in IRAF⁴ and optimally extracted apertures with the *apall* function. Some echelle orders were discarded due to CCD fringing, heavy contamination from sky emission and telluric absorption features, cross-disperser order overlap, and low throughput. For HRS (MRS), we kept a total of 48 (14) orders covering

TABLE 1
SUMMARY OF SPECTROSCOPIC OBSERVATIONS

Target	Telescope/Instrum.	N _{obs}	Year
PG 1449+653	HET/HRS	7	2012–2013
	HET/MRS	8	2005–2008
	MMT/Blue Spect.	5	1997
PG 1701+359	HET/HRS	8	2012–2013
	HET/MRS	13	2005–2008
	MMT/Blue Spect.	8	1997, 2002–2003

4100–7000 Å (4400–6200 Å).

We supplement the HET data with single-order, long-slit spectra from the Blue Spectrograph at the Multi Mirror Telescope (MMT) obtained in 1997 and from 2002 to 2003. An 832 mm⁻¹ grating was used in second order to achieve wavelength coverage of 4000–4950 Å at a resolution of 1.1 Å ($R = 4100$) and dispersion near 0.36 Å pixel⁻¹. MMT data were reduced using the same IRAF routines mentioned above for the HET observations. Table 1 summarizes the entire data set.

3. ANALYSIS

We generally followed the same procedures outlined in Paper I to measure radial velocities (RVs) and determine the best-fitting orbital parameters for each system; we highlight only certain aspects of these procedures here (along with any deviations from Paper I) and refer readers to Paper I for full disclosure of our analysis methods.

3.1. Companion classification

We cross-correlated the PG 1449+653 and PG 1701+359 spectra with MS standards (F0–K7) observed by the MMT and HET in the same instrumental configurations as our data. IRAF's *fxcor* routine was used for all regions of the spectra except those around the hydrogen Balmer and helium lines. We determined the best-matching MS spectra for each target from the Tonry–Davis ratio (R -value output from *fxcor*; Tonry & Davis 1979) and the *fxcor*-outputted velocity errors for each template. A spectral type of G0V was consistently found for PG 1449+653. The PG 1701+359 spectrum, which has lower S/N and higher dilution, was best-matched to a K0V standard, although several G-type standards (as early as G0V) also fit the spectra reasonably well.

We also adopt the approach used by Stark & Wade (2003) to photometrically determine the spectral types of the cool companions. After correcting for reddening (Schlegel et al. 1998), we compare the colors of PG 1449+653 and PG 1701+359 to a theoretical grid of $B-V$ and $J-K$ colors for hot subdwarf binaries with cool main sequence companions. We note that Population I colors were assumed for the cool companions, although kinematics suggest these systems might have halo-like orbits (§5). For each pairing, the dilution factor of the companion spectrum in the V -band ($D_V \equiv L_{\text{comp}}/L_{\text{total}}$) was varied from 1–100%. Color indices for the cool companions and hot subdwarfs are taken from Johnson (1966) and Stark & Wade (2003), respectively. For PG 1449+653, we find colors consistent with a 'typical' hot subdwarf star and a F8–G3 dwarf (best fit: G1) with a dilution factor around $D_V \sim 0.3$; these results agree with the spectroscopically-determined value. PG 1701+359's

⁴ IRAF is distributed by the National Optical Astronomy Observatories, which are operated by the Association of Universities for Research in Astronomy, Inc., under cooperative agreement with the National Science Foundation

TABLE 2
HELIOCENTRIC RADIAL VELOCITIES OF THE COOL COMPANION

HJD -2450000	RV _{MS} [km s ⁻¹]	Facility	HJD -2450000	RV _{MS} [km s ⁻¹]	Facility
PG 1449+653			PG 1701+359		
511.0187	-128.4 ± 1.0	MMT	627.8929	-121.0 ± 1.9	MMT
626.8101	-129.3 ± 1.3	MMT	633.8716	-123.3 ± 1.9	MMT
627.7691	-129.1 ± 1.0	MMT	642.8422	-122.2 ± 1.9	MMT
642.7782	-129.3 ± 1.0	MMT	643.7559	-124.8 ± 1.8	MMT
701.6427	-130.6 ± 1.4	MMT	701.6934	-122.9 ± 2.0	MMT
3462.8508	-136.0 ± 0.8	HET/MRS	1654.7222	-119.6 ± 1.1	MMT
3479.8705	-136.4 ± 1.0	HET/MRS	2544.6458	-123.0 ± 1.7	MMT
3503.8035	-138.0 ± 0.9	HET/MRS	2826.8606	-123.9 ± 1.6	MMT
3520.6751	-138.4 ± 0.8	HET/MRS	3482.8107	-122.2 ± 1.2	HET/MRS
3758.0254	-143.5 ± 0.7	HET/MRS	3520.9447	-122.4 ± 0.9	HET/MRS
3827.9095	-138.4 ± 1.1	HET/MRS	3543.8831	-123.8 ± 1.3	HET/MRS
3855.8400	-138.3 ± 1.2	HET/MRS	3584.7790	-123.6 ± 1.1	HET/MRS
4216.8374	-128.5 ± 0.8	HET/MRS	3609.7073	-122.8 ± 1.6	HET/MRS
5991.9222	-128.4 ± 0.2	HET/HRS	3827.8767	-120.4 ± 1.3	HET/MRS
6018.8438	-128.5 ± 0.2	HET/HRS	3854.7918	-119.0 ± 1.3	HET/MRS
6061.6989	-129.5 ± 0.2	HET/HRS	4273.8819	-122.1 ± 1.2	HET/MRS
6086.6883	-130.2 ± 0.2	HET/HRS	4506.0149	-121.3 ± 0.9	HET/MRS
6118.6349	-131.1 ± 0.2	HET/HRS	4569.8307	-117.1 ± 2.9	HET/MRS
6334.9466	-142.6 ± 0.2	HET/HRS	4582.7928	-118.8 ± 0.8	HET/MRS
6376.9266	-144.2 ± 0.2	HET/HRS	4612.7189	-117.1 ± 1.5	HET/MRS
...	4671.7919	-115.3 ± 1.4	HET/MRS
...	5997.8963	-121.0 ± 0.4	HET/HRS
...	6040.7881	-119.9 ± 0.2	HET/HRS
...	6068.9367	-118.7 ± 0.3	HET/HRS
...	6098.6339	-117.6 ± 0.2	HET/HRS
...	6145.7336	-116.9 ± 0.2	HET/HRS
...	6191.6229	-116.2 ± 0.3	HET/HRS
...	6326.0072	-118.3 ± 0.3	HET/HRS
...	6370.8962	-119.5 ± 0.3	HET/HRS

composite colors imply a G7–K2 dwarf companion (best fit: K0) with $D_V \sim 0.15$, also consistent with the observed composite spectrum.

3.2. Radial velocity measurements

Helio-centric radial velocities were determined by cross-correlating each spectrum against velocity standards using IRAF’s *fxcor* and *rvcorrect* routines. All MMT spectra were correlated against the velocity standard HD 39587, a G0V dwarf, which was observed using the same instrumental setup as our target observations. For the HET data, we achieve the best results when using a single, high S/N twilight sky spectrum as the correlation template for all HRS and MRS observations. We extracted HET velocities from each order individually, being sure to avoid spectral regions where subdwarf features compromise our ability to measure the cool companion velocities. We adopt as the error the standard deviation of the mean of the order-by-order velocity fits. Typical velocity errors ranged from 1–1.5 km s⁻¹ for MRS, 200–400 m s⁻¹ for HRS, and 1–1.5 km s⁻¹ for the MMT spectra. Table 2 presents all cool companion velocities and their associated errors.

We attempted to measure the orbital reflex motion of the hot subdwarf in each system by examining the positions of He I & He II absorption profiles. We avoided using the sdB’s H Balmer lines as they are contaminated by narrower Balmer lines from the cool companion (and

TABLE 3
HELIOCENTRIC RADIAL VELOCITIES
OF THE SDB IN PG 1449+653

HJD -2450000	RV _{MS} [km s ⁻¹]	Facility
3462.8508	-129.9 ± 5.0	HET/MRS
3479.8705	-130.5 ± 6.0	HET/MRS
3503.8035	-130.3 ± 5.6	HET/MRS
3520.6751	-124.5 ± 5.0	HET/MRS
3758.0254	-122.3 ± 3.9	HET/MRS
3827.9095	-122.5 ± 6.6	HET/MRS
3855.8400	-128.3 ± 7.2	HET/MRS
4216.8374	-135.3 ± 4.7	HET/MRS
5991.9222	-146.9 ± 3.3	HET/HRS
6018.8438	-142.5 ± 2.9	HET/HRS
6061.6989	-144.4 ± 3.8	HET/HRS
6086.6883	-140.8 ± 2.9	HET/HRS
6118.6349	-137.7 ± 2.9	HET/HRS
6334.9466	-120.2 ± 3.0	HET/HRS
6376.9266	-119.9 ± 3.1	HET/HRS

in the MRS/HRS spectra, they are broader than the wavelength coverage of individual echelle orders). For PG 1449+653, we extracted RVs by cross-correlating the He I 5875 Å profile in each spectrum against a self template, chosen to be the highest S/N spectrum obtained. The template’s zero point was determined by cross-

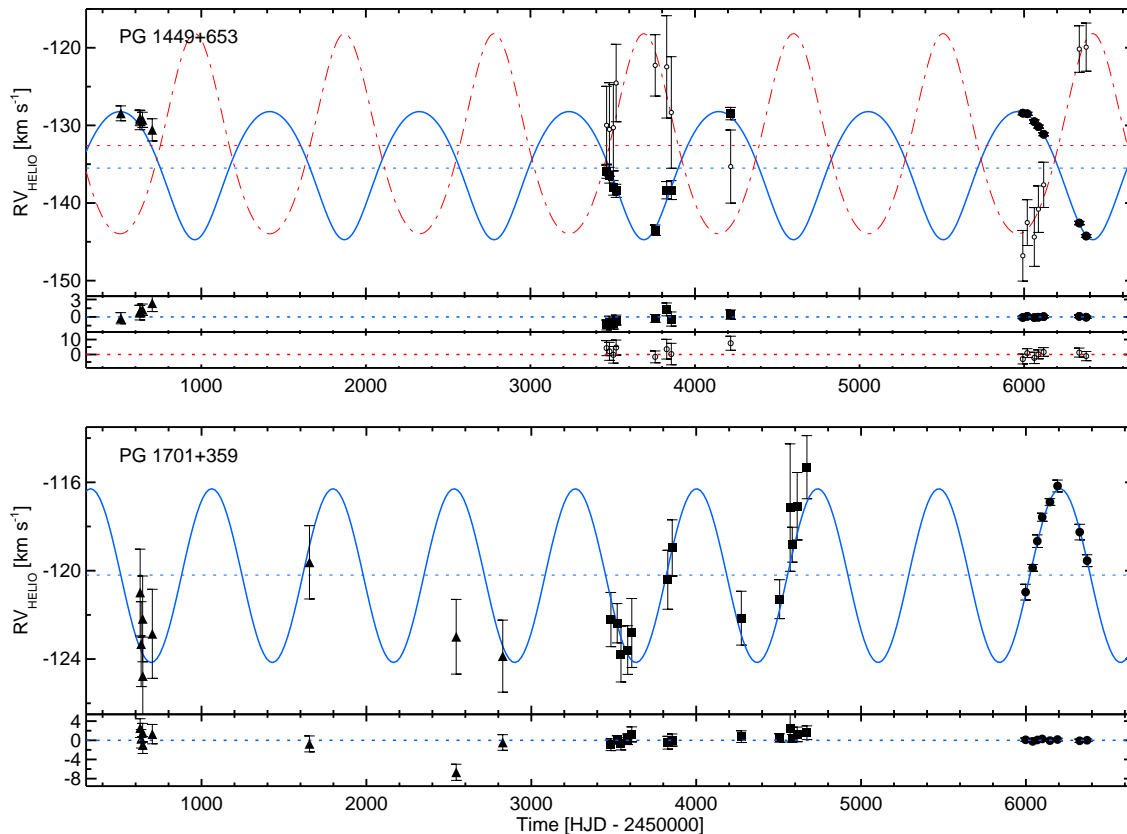


FIG. 1.— Heliocentric radial velocities of PG 1449+653 (top panel) and PG 1701+359 (bottom panel). Cool companion measurements from HET/MRS, HET/HRS, and MMT/Blue Spectrograph are shown with filled circles, squares, and triangles, respectively. Open circles in the top panel mark the sdB velocities measured from He lines in the HET spectra. Some of the error bars are difficult to see as they are smaller than the symbols. The best-fitting circular orbital solutions for the sdB and cool companion are denoted with dot-dashed (orange) and solid (blue) lines, respectively. Residuals from this fit are shown in the lower portions of the panels for the cool companion and, for PG 1449+653, the hot subdwarf. (A color version of this figure is available in the online journal.)

correlating the template against an sdB model spectrum with $T_{\text{eff}} = 30000$ K and $\log g = 5.58$. This synthetic template includes pressure broadening and asymmetry in the 5875 \AA He I multiplet. Table 3 summarizes the sdB velocities measured from all HET spectra. Unfortunately, our efforts to extract precise sdB velocities were futile in the case of PG 1701+359. This shortcoming likely results from a combination of a lower S/N in many of the spectra (due to shorter exposure times) and intrinsically weaker He I lines, which could result from the sdB in PG 1701+359 having a significantly different photospheric helium abundance and/or effective temperature than the sdB in PG 1449+653. We also note that the orbital velocities associated with PG 1701+359 are more than a factor of two smaller than those of PG 1449+653 and, naturally, harder to detect.

3.3. Determining the orbital parameters

We solved for the full set of orbital parameters (P , K , e , ω , γ , T_0) using the IDL-based RVLIN software (Wright & Howard 2009) and estimated parameter uncertainties using a RVLIN-drive bootstrapping technique (Wang et al. 2012). After first running the code with eccentricity (e) fixed to zero, we refitted the data with it and the argument of periastron (ω) left adjustable. We also allowed RVLIN to freely fit any zero-point offsets between the MMT, MRS/HET, and HRS/HET velocities,

but as no significant shifts were found, we ultimately set the offsets to zero. To be certain RVLIN converged on the global minimum, we computed a ‘floating-mean periodogram’ (Cumming et al. 1999) for each RV curve to investigate χ^2 as a function of period. During this process, a series of sine waves are fitted to the data with adjustable amplitudes and periods ranging from 0.1 to 10000 d (in steps of $\log P[\text{d}] = 0.001$). Only one probable period emerges from the periodogram for each target; the next-largest alias peaks are 10^3 times less probable. These periods also correspond to the global minima found by RVLIN, and so we are confident we have found the correct periods.

4. THE ORBITAL SOLUTIONS

Figure 1 and Table 4 present the velocity curves and best-fitting orbital parameters for PG 1701+359 and PG 1449+643, which we discuss in detail below.

4.1. PG 1449+653

The abundance of absorption features from the early G dwarf provided robust RV measurements with mean errors ranging from 245 m s^{-1} (HRS/HET) to 1400 m s^{-1} (MMT). Measuring the reflex motion of the sdB proved more difficult as most of the subdwarf’s absorption features (H Balmer lines, He I lines) were heavily contaminated by features from the cool companion and could not provide reliable velocity estimates. We were only able to

TABLE 4
ORBITAL PARAMETERS

Target	P [d]	T_0^a [HJD-2450000]	e	ω [deg]	K_{MS} [km s $^{-1}$]	K_{sdB} [km s $^{-1}$]	γ [km s $^{-1}$]
PG 1449+653	909 \pm 2	3675 \pm 35	0.11 \pm 0.02	174 \pm 15	8.2 \pm 0.3	12.8 \pm 1.1	-135.5 \pm 0.2
	908 \pm 2	3251 \pm 40	0.0 (fixed)	...	8.3 \pm 0.2	13.5 \pm 0.8	-136.4 \pm 0.2
PG 1701+359	738 \pm 4	3869 \pm 80	0.07 \pm 0.04	298 \pm 38	3.6 \pm 0.2	...	-120.1 \pm 0.2
	734 \pm 3	3269 \pm 60	0.0 (fixed)	...	3.9 \pm 0.2	...	-120.2 \pm 0.2

^aTime of velocity maximum (maximum redshift) in the cool companion RV curve ($e = 0$ case) or time of periastron passage ($e \neq 0$).

TABLE 5
COORDINATES, VELOCITIES, AND DISTANCE ESTIMATES

Target	RA [J2000]	Dec [J2000]	$\mu_\alpha \cos \delta^a$ [mas yr $^{-1}$]	μ_δ^a [mas yr $^{-1}$]	γ [km s $^{-1}$]	d^b [kpc]
PG 1449+653	14:50:36.1	+65:05:53	-21.7 \pm 2.1	13.6 \pm 1.0	-135.5 \pm 0.2	0.98 \pm 0.16
PG 1701+359	17:03:21.6	+35:48:49	-57.9 \pm 4.0	20.4 \pm 0.9	-120.2 \pm 0.2	0.69 \pm 0.15
PG 1104+243	11:07:26.3	+24:03:12	-65.9 \pm 1.2	-25.1 \pm 1.2	-15.68 \pm 0.05	0.33 \pm 0.11
PG 1317+123	13:19:53.6	+12:03:59	-6.9 \pm 1.1	-1.6 \pm 1.1	+40.3 \pm 0.2	0.33 \pm 0.11
PG 1338+611	13:40:14.7	+60:52:48	14.5 \pm 0.9	-61.4 \pm 0.8	+32.58 \pm 0.07	0.32 \pm 0.11

^aproper motions taken from UCAC4 (Zacharias et al. 2012)

^bcalculated from the distance modulus assuming a 'typical' sdB star and our best estimate of the companion's spectral type; error bars are conservative.

extract velocities from the HET data, using the 5875 Å He I line alone. This feature, which is significantly diluted due to continuum from the companion, appears in two adjacent orders in the MRS spectra, but only in one order in the HRS data. Using the methods described in §3.2, we were able to extract sdB RVs with errors ranging from 3–7 km s $^{-1}$.

The top panel of Figure 1 presents the MS and sdB velocity curves, which are 180 degrees out of phase, as expected for a binary system. Given the relatively large uncertainties on the sdB measurements, we used only the MS velocities to determine the orbital parameters with RVLIN. Table 4 lists the results for the best-fitting circular and elliptical orbits. To determine whether the eccentric solution is preferred, we apply the revised Lucy–Sweeney (LS) test (Lucy 2012; Lucy & Sweeney 1971), which uses Bayes' theorem to determine bounds on the exact eccentricity using the value $e \pm \mu$ we measured from RVLIN. According to the LS test, we can reject the circular orbit solution in favor of an eccentric orbit with $e = 0.11 \pm 0.03$. For the remainder of the text, we continue under the assumption of an eccentric orbit, for which we report $P = 909 \pm 2$ d.

To derive the mass ratio, we also measured the semi-amplitude of the sdB RV curve. We fixed the period, eccentricity, and phase to the values determined from the cool companion measurements (the phase was shifted by 180 deg) and allowed the semi-amplitude and systemic velocity to float freely. Allowing γ to adjust accounts for a difference in the surface gravities (gravitational redshifts) of the two components, which results in apparent systemic velocities that differ from one another. In sdB+F/G/KV systems, this difference can reach upwards of 2 km s $^{-1}$ and was first measured for a hot subdwarf binary by Vos et al. (2012). We find $K_{\text{sdB}} = 12.8 \pm 1.0$ km s $^{-1}$ and $\gamma_{\text{sdB}} = -132.6 \pm 1.1$ km s $^{-1}$ for the sdB star. The measured difference in systemic velocities

is $\Delta\gamma = 2.9 \pm 1.1$ km s $^{-1}$. This measurement, when combined with a $\log g$ estimate for the main sequence companion, allows one to compute the gravitational redshift (and thus, $\log g$) for the hot subdwarf star, but in this case the errors are too large to make this a fruitful exercise.

From K_{MS} and K_{sdB} , we calculate a mass ratio of $q = 0.64 \pm 0.06$, where $q \equiv K_{\text{MS}}/K_{\text{sdB}}$. If we assume $M_{\text{MS}} = 1.04 \pm 0.12 M_\odot$ for the cool companion (based on our spectroscopic classification, which assumes solar abundances), we derive a subdwarf mass of $M_{\text{sdB}} = 0.66 \pm 0.10 M_\odot$. With this precision, we cannot claim a significant deviation from the canonical mass value ($\sim 0.5 M_\odot$).

4.2. PG 1701+359

Heavy dilution of the cool companion's spectral features from the hot subdwarf's continuum made classifying the PG 1701+359 spectrum and measuring velocities more difficult than in the case of PG 1449+653. Errors on the cool companion RVs ranged from 250 m s $^{-1}$ (HRS) to 1–2 km s $^{-1}$ (MRS, MMT). We were not able to derive useful sdB velocities from the He I lines. In view of the expected acceleration, which is much smaller than in the PG 1449+653 case, they are too weak for our cross-correlation measurement technique to achieve the required precision.

The cool companion RV curve (bottom panel, Figure 1) exhibits a small-amplitude variation (~ 4 km s $^{-1}$) with a period near 2.0 years. Although an eccentric solution models our data more accurately (naturally), we cannot yet rule out a circular orbit since the best-fitting $e = 0.07 \pm 0.04$ solution was rejected by the revised LS test. Instead, we replace our measured value with an upper limit, $e \leq 0.23$, which was determined using their recommended prescription (Appendix 2 of Lucy 2012). The derived orbital parameters from the circular and

non-circular models agree with one another to within the errors. Our current phase coverage is incomplete as nearly all of our velocities are on the ascending portion of the RV curve; additional measurements on the descending slope will greatly improve the eccentricity estimate. We continue under the assumption of $e = 0$, for which we report $P = 734 \pm 3$.

5. GALACTIC KINEMATICS

Both PG 1449+653 and PG 1701+359 display relatively large systemic velocities, so we have calculated their Galactic trajectories to see what conclusions can be drawn concerning their kinematic population (halo vs. thick disk vs. thin disk). We also include as a comparison an analysis of the three systems solved in Paper I (PG 1104+243, PG 1317+123, & PG 1338+611), which were found to have less interesting space motions. A kinematical study requires the full set of 6-D phase space coordinates, which we determine from the right ascension (α), declination (δ), distance (d), systemic velocity (γ), and proper motion ($\mu_\alpha \cos \delta$, μ_δ). We summarize these input parameters in Table 5.

We adopt the values of γ shown in Table 4 as the systemic velocity inputs ($e=0.11$ solution for PG 1449+653, $e=0$ solution for PG 1701+359). Proper motion measurements with errors ranging from 3–11 mas yr⁻¹ were taken from the Fourth U.S. Naval Observatory CCD Astroglyph Catalog (UCAC4; Zacharias et al. 2012). The most difficult parameter to determine is the distance. Here we estimate a range of probable line-of-sight distances to each binary from the distance moduli. We assume $T_{\text{eff}} = 24000\text{--}38000$ K and $R = 0.15\text{--}0.22 R_\odot$ for the sdB, taking into account conventional correlations between these parameters for hot subdwarfs. For the cool companion, we assume solar abundances and use main sequence temperatures and radii corresponding to our spectral classifications. These values define absolute Visual magnitudes, which were compared to the apparent Visual magnitudes and, after taking into account the measured dilution of the cool companion (§3.1) and the extinction (Schlegel et al. 1998), provided us with the rough distance estimates shown in Table 5.

We converted positions and motions to Galactocentric coordinates⁵ (X , Y , Z) and velocities (U , V , W), adopting a Galactocentric distance of 8.5 kpc for the Sun. The resulting 6-D phase space coordinates are presented in Table 6. We also include in this table the velocity component in the direction of Galactic rotation (Θ), the component towards the center of the Galaxy (Φ), and the angular momentum (I_z). The space velocities were transformed to the Local Standard of Rest by removing a solar motion of (10.0, 5.3, 7.2) km s⁻¹ (Dehnen & Binney 1998). We used the ORBIT6 code developed by Odenkirchen & Brosche (1992) to calculate the orbits of the binaries in the axisymmetric Galactic potential of Allen & Santillan (1991). In this model, the disk rotation speed and volume density are 220 km s⁻¹ and 0.15 M_⊙ pc⁻³, respectively. We reconstructed the path of each system over a 10 Gyr period with time steps of 1 Myr in order to obtain a clear picture of the

shape of each orbit. Figure 2 shows the resulting trajectories in the Y - X , Z - X , and Z - ρ planes. The last four columns of Table 6 list the apo- and perigalactic distances (R_a and R_p respectively), the maximum Z -direction excursion from the disk, and the eccentricity ($e \equiv (R_a - R_p)/(R_a + R_p)$), all of which were determined by integrating the orbits.

Figure 2 reveals the orbits of PG 1449+653 and PG 1701+359 to be fundamentally different from those of the other systems. Whereas PG 1104+243, PG 1317+123, and PG 1338+611 exhibit relatively well-behaved, disk-like trajectories that never stray far from the Galactic plane (PG 1317+123 being the most Sun-like), the orbits of PG 1449+653 and PG 1701+359 are significantly more eccentric and carry these systems much farther out of the disk. The orbit of PG 1701+359 shows surprisingly little angular momentum, with a highly-eccentric orbit ($e \sim 0.8$) bringing it as close as 1.5 kpc to the Galactic center and as far away as 10.6 kpc. PG 1449+653 currently appears to be near apogalacticon. We remind the reader that all of the orbits calculated here represent *approximate* trajectories; small changes in the initial 6D phase-space coordinates can significantly change the results, in addition to any encounters with localized regions of higher density in the Galaxy which are not accounted for by ORBIT6.

We employ the method described in the appendix of Grether & Lineweaver (2007) to calculate the probabilities that each system belongs to the halo (P_{halo}), thick disk (P_{thick}), or thin disk (P_{thin}). This procedure assumes that all stellar systems belong to one of these three subpopulations, and that the Galactic velocities (U, V, W) and metallicities ($[\text{Fe}/\text{H}]$) of each subpopulation follow Gaussian distributions defined by the data in Table 4 of Robin et al. (2003). Since we lack precise metallicity estimates for the two systems studied here, we plot these probabilities in Figure 3 over a broad range of metallicities.

The kinematics alone are enough to rule out thin disk membership for both PG 1449+653 and PG 1701+359. Choosing between the thick disk and halo populations will ultimately require precise measurements of the metallicity. If $[\text{Fe}/\text{H}]$ turns out to be much less than -1.55 (-1.25), PG 1449+653 (PG 1701+359) would most likely be a member of the Galactic halo and not the thick disk. Vos et al. (2012) report $[\text{Fe}/\text{H}] = -0.58 \pm 0.11$ dex for PG 1104+243; using this value and the system’s kinematics, we find that there is $\sim 94\%$ probability it is a member of the thick disk. We cannot assign memberships to PG 1317+123 and PG 1338+611 at this time using the data currently available.

The only major 3D kinematical study of hot subdwarfs in the Galaxy was carried out by Altmann et al. (2004) on a sample of 114 stars selected primarily from the Hamburg/ESO (HE) and Palomar Green (PG; Green et al. 1986) surveys; some of their targets were composite-spectra systems. They found that the vast majority of sdBs are members of the disk, while only a minority ($\sim 15\%$) appear to be halo objects. Of the disk population, the thick disk seems to be preferred over the thin disk. We cannot make any definitive claims concerning Galactic membership differences between the composite-spectra systems and the apparently single or short-period sdB binaries at this time, owing to the small

⁵ Left-handed Cartesian coordinates where X increases from Galactic center to anti-Solar direction and Z increases towards the Galactic North Pole.

TABLE 6
GALACTOCENTRIC 6-D PHASE SPACE COORDINATES AND ORBITAL PARAMETERS

Target	X [kpc]	Y [kpc]	Z [kpc]	U [km s $^{-1}$]	V [km s $^{-1}$]	W [km s $^{-1}$]	Φ [km s $^{-1}$]	Θ [km s $^{-1}$]	I_z [kpc km s $^{-1}$]	R_a [kpc]	R_p [kpc]	z_{\max} [kpc]	e
PG 1449+653	-8.67	+0.64	+0.73	-78	+101	-81	+10	+95	-829	2.61	9.91	3.73	0.58
PG 1701+359	-8.21	+0.46	+0.41	-132	+68	+94	+11	+60	-492	1.48	10.69	4.70	0.76
PG 1104+243	-8.61	-0.07	+0.30	-59	+168	-51	+9.9	+168	-1447	5.25	9.37	1.12	0.28
PG 1317+123	-8.42	-0.05	+0.31	+11	+219	+46	+8.7	+219	-1843	8.23	8.88	0.87	0.04
PG 1338+611	-8.56	+0.14	+0.22	+62	+216	+72	+7.9	+210	-1797	6.96	11.16	2.21	0.23

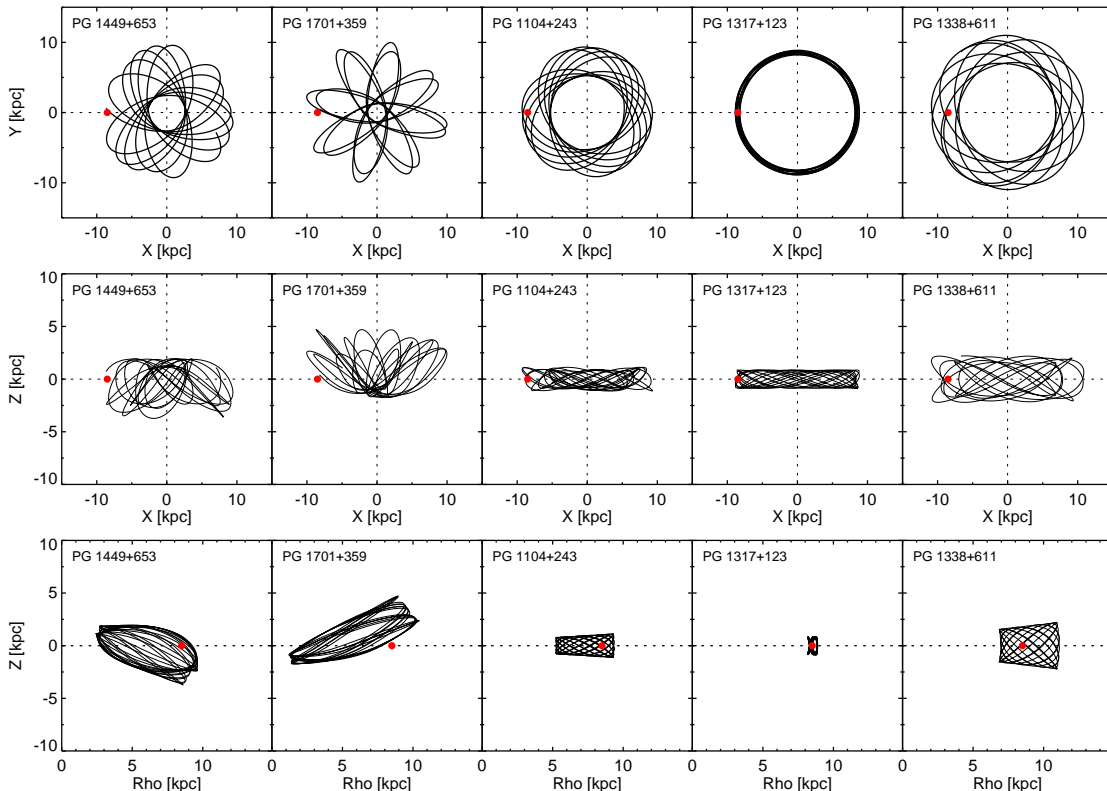


FIG. 2.— Galactocentric orbits for PG 1449+653, PG 1701+359, and the three binaries solved in Paper I, shown over a 10 Gyr period. Orbits were calculated using the potential of Allen & Santillan (1991). The top two rows show the orbits in the Y - X and Z - X planes, while the bottom row shows the height above the disk (Z) as a function of Galactocentric distance (Rho). In each panel, the location of the Sun is marked with a solid red circle, for reference. (A color version of this figure is available in the online journal.)

number of long-period systems currently studied in sufficient detail. Eventually, a kinematical analysis of a larger sample of composite-spectra binaries, aided by precise proper motion measurements from *Gaia*, might provide additional insight into the formation scenarios of long-period binaries. As some of these binaries show peak-to-peak RV amplitudes in excess of 15 km s $^{-1}$, it is imperative that such studies use the true systemic velocity when computing Galactic trajectories, as determined from a well-sampled RV curve with full phase coverage.

6. CONCLUDING REMARKS

We have presented follow-up spectroscopic observations of the sdB+G/K binaries PG 1449+653 and PG 1701+359, the tenth and eleventh such systems for which orbital parameters have been determined. Combining spectroscopic data from the MMT and HET, we find orbital periods around two years for both binaries. While

we cannot claim an eccentric orbit in the case of PG 1701+359, PG 1449+653 appears to have a mildly eccentric orbit, thereby joining PG 1338+611 (Paper I) and possibly PG 1018+243 (Deca et al. 2012) in an emerging group of long-period sdB+/F/G/K binaries with non-circular orbits. If wide sdB binaries continue to show eccentric orbits, this would suggest one of the following possibilities: (1) these systems are or were hierarchical triple-star systems, (2) circularization was never achieved because the sdB progenitor did not fill its Roche lobe, or (3) one of several possible mechanisms pumped eccentricity into the system. Further details concerning eccentric orbits of sdB+F/G/K binaries and the implications thereof are discussed in Paper I. A kinematical analysis inspired by the relatively large systemic velocities found for each system shows that they are probably not members of the Galactic thin disk; we cannot yet distinguish between thick-disk or halo memberships.

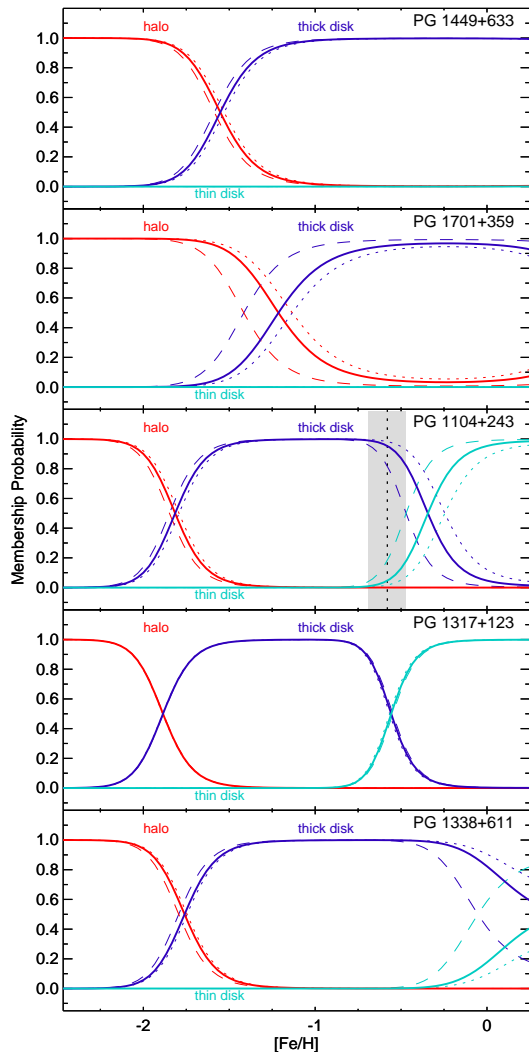


FIG. 3.— Galactic membership probabilities for PG 1449+633 and PG 1701+359 (top two panels). The solid red, dark blue, and light blue lines denote the probabilities that each system is a member of the halo, thick disk, and thin disk, respectively, for a range of metallicities, using our best estimate for the distance. The dotted and dashed lines show how these probabilities change when we modify the distance to accommodate the uncertainties shown in Table 5. The kinematics alone show it is unlikely either system is a member of the Galactic thin disk. In the bottom three panels, we present the membership probabilities for the three binaries solved in Paper 1. The vertical line and shaded region in the PG 1104+243 panel represent the $[\text{Fe}/\text{H}]$ measurement and associated uncertainty reported by Vos et al. (2012). (A color version of this figure is available in the online journal.)

Our results continue the trend of finding long periods (on the order of years) for hot subdwarf stars with G/K-type main sequence companions. Binary population synthesis codes (e.g., Han et al. 2002, 2003) are relatively successful at matching the observed orbital periods of sDBs with M dwarf or white dwarf companions but struggle to reproduce the long periods found for sDB+F/G/KV systems. Even though relatively few of these long-period binaries have been studied to date, current observations strongly suggest that (1) the assumptions made in some hot subdwarf formation scenarios should be revised and (2) some of the parameterizations in BPS models be re-tuned. As demonstrated by Clausen et al. (2012), subtle variations in the assumptions about the minimum core mass required for helium ignition, the envelope binding energy, the criteria for stable mass transfer, and the amount of mass lost during stable mass transfer can lead to BPS models producing significantly different distributions of orbital properties for hot subdwarf binaries. Orbital parameters for many more sDB+F/G/KV systems must be measured in order to thoroughly evaluate the predictive success of current BPS models and determine which parameterizations and assumptions must be adjusted to match the empirical period distribution.

This material is based upon work supported by the National Science Foundation under Grant No. AST-0908642. We thank Rohit Deshpande and Suvrath Mahadevan for providing HRS/HET spectra of MS stars and Eva Ziegerer for providing a copy of the ORBIT6 code. The Hobby-Eberly Telescope is a joint project of the University of Texas at Austin, the Pennsylvania State University, Stanford University, Ludwig-Maximilians-Universität München, and Georg-August-Universität Göttingen. The HET is named in honor of its principal benefactors, William P. Hobby and Robert E. Eberly. This research has made use of NASA’s Astrophysics Data System Bibliographic Services and the SIMBAD database, operated at CDS, Strasbourg, France.

Facilities: HET (MRS, HRS), MMT (Blue Spectrograph)

REFERENCES

- Allen, C., & Santillan, A. 1991, *RevMexAA*, 22, 255
 Altmann, M., Edelmann, H., & de Boer, K. S. 2004, *A&A*, 414, 181
 Barlow, B. N., Wade, R. A., Liss, S. E., Østensen, R. H., & Van Winckel, H. 2012, *ApJ*, 758, 58 (Paper I)
 Brown, T. M., Bowers, C. W., Kimble, R. A., Sweigart, A. V., & Ferguson, H. C. 2000, *ApJ*, 532, 308
 Clausen, D., & Wade, R. A. 2011, *ApJ*, 733, L42
 Clausen, D., Wade, R. A., Kopparapu, R. K., & O’Shaughnessy, R. 2012, *ApJ*, 746, 186
 Cumming, A., Marcy, G. W., & Butler, R. P. 1999, *ApJ*, 526, 890
 Deca, J., Marsh, T. R., Østensen, R. H., et al. 2012, *MNRAS*, 421, 2798
 Dehnen, W., & Binney, J. J. 1998, *MNRAS*, 298, 387
 Geier, S., Hirsch, H., Tillich, A., et al. 2011, *A&A*, 530, A28
 Green, E. M., Fontaine, G., Hyde, E. A., Charpinet, S., & Chayer, P. 2006, *Baltic Astronomy*, 15, 167
 Green, R. F., Schmidt, M., & Liebert, J. 1986, *ApJS*, 61, 305
 Greenstein, J. L., & Sargent, A. I. 1974, *ApJS*, 28, 157
 Grether, D., & Lineweaver, C. H. 2007, *ApJ*, 669, 1220
 Han, Z., Podsiadlowski, P., Maxted, P. F. L., & Marsh, T. R. 2003, *MNRAS*, 341, 669
 Han, Z., Podsiadlowski, P., Maxted, P. F. L., Marsh, T. R., & Ivanova, N. 2002, *MNRAS*, 336, 449
 Heber, U. 1986, *A&A*, 155, 33
 Johnson, H. L. 1966, *ARA&A*, 4, 193

- Liebert, J., Saffer, R. A., & Green, E. M. 1994, *AJ*, 107, 1408
- Lucy, L. B. 2012, *A&A*, 551, 47
- Lucy, L. B., & Sweeney, M. A. 1971, *AJ*, 76, 544
- Mengel, J. G., Norris, J., & Gross, P. G. 1976, *ApJ*, 204, 488
- Moni Bidin, C., & Piotto, G. 2010, *Ap&SS*, 329, 19
- Napiwotzki, R. 2008, in *Astronomical Society of the Pacific Conference Series*, Vol. 391, *Hydrogen-Deficient Stars*, ed. A. Werner & T. Rauch, 257
- Nelemans, G. 2010, *Ap&SS*, 329, 25
- Odenkirchen, M., & Brosche, P. 1992, *Astronomische Nachrichten*, 313, 69
- Østensen, R. H., & Van Winckel, H. 2012, in *ASP Conf. Ser. 452, Fifth Meeting on Hot Subdwarf Stars and Related Objects*, ed. D. Kilkenney, C. S. Jeffery, & C. Koen, (San Francisco, CA: ASP), 163
- Ramsey, L. W., Adams, M. T., Barnes, T. G., et al. 1998, *Proc. SPIE*, 3352, 34
- Robin, A. C., Reylé, C., Derrière, S., & Picaud, S. 2003, *A&A*, 409, 523
- Saffer, R. A., Green, E. M., & Bowers, T. 2001, in *ASP Conf. Ser. 226, 12th European Workshop on White Dwarfs*, ed. J. L. Provençal, H. L. Shipman, J. MacDonald, & S. Goodchild (San Francisco, CA: ASP), 408
- Saffer, R. A., Bergeron, P., Koester, D., & Liebert, J. 1994, *ApJ*, 432, 351
- Schlegel, D. J., Finkbeiner, D. P., & Davis, M. 1998, *ApJ*, 500, 525
- Stark, M. A., & Wade, R. A. 2003, *AJ*, 126, 1455
- Tonry, J., & Davis, M. 1979, *AJ*, 84, 1511
- Vos, J., Østensen, R. H., Degroote, P., et al. 2012, *A&A*, 548, A6
- Wang, X., Sharon, Wright, J. T., Cochran, W., et al. 2012, *ApJ*, 761, 46
- Wright, J. T., & Howard, A. W. 2009, *ApJS*, 182, 205
- Zacharias, N., Finch, C. T., Girard, T. M., Henden, A., et al. 2012, *VizieR Online Data Catalog*, I/322